3. Cowper G.R., Symonds P.S., "Strain hardening and strain rate effects in the impact loading of cantilever beams", Applied Mathematics Report No. 28, Brown University, Providence, Rhode Island, USA, 1957.
4. Giovino G., Olmati P., Garbati S., Bontempi F., "Blast resistance assessment of concrete wall panels: experimental and numerical investigations", *International Journal of Protective Structure,* V. 5, No. 3, 2014, pp. 349-366.
5. Hao Y., Hao H., Li Z.X., "Numerical analysis of lateral inertial confinement effects on impact test of concrete compressive material properties", *International Journal of Protective Structures*, V. 1, No. 1, 2010, pp. 145-168.
6. Livermore Software Technology Corporation, "LS-DYNA theory manual", California, US, 2012.
7. Malvar L.J., Ross C.A., "Review of Strain Rate Effects for Concrete in Tension", *ACI Materials Journal*, V. 95, No. 6, 1998, pp. 735-739.
8. Murray Y.D., "User's Manual for LS-DYNA Concrete Material Model 159", FHWA-HRT-05-062, 2007.
9. Naito, C., Ren, R., "An evaluation method for precast concrete diaphragm connectors based on structural testing", *PCI Journal*, V. 58, No. 2, No. , 2013, pp 106-118.
10. Naito C.J., Hoemann J., Beacraft M., Bewick B., "Performance and characterization of shear ties for use in insulated precast concrete sandwich wall panels", *Journal of Structural Engineering*, V. 138, 2012, pp. 1-11.
11. Naito C., Olmati P., Trasborg P., Davidson J., Newberry C., "Assessment of insulated concrete walls to close-in blast demands", *Journal of Performance of Constructed Facilities,* 2014, http://ascelibrary.org/doi/abs/10.1061/(ASCE)CF.1943-5509.0000643.
12. NCHRP, "Blast-resistant highway bridges: design and detailing guidelines", National Cooperative Highway Research Program United States of America, Washington DC, 2009.
13. Popovics S., "A Numerical Approach to the Complete Stress Strain Curve for Concrete", *Cement and Concrete Research*, V. 3, No. 5, 1973, pp. 583-599.
14. Schenker A., Anteby I., Gal E., Kivity Y., Nizri E., Sadot O., Michaelis R., Levintant O., Ben-Dor G., "Full-scale field tests of concrete slabs subjected to blast loads", *International Journal of Impact Engineering*, V. 35, 2008, pp. 184-198.
15. Thiagarajan G., Vasudevan A.K., Robert S., "Numerical modeling of concrete slabs reinforced with high strength low alloy vanadium steel bars subjected to blast loads", *ACI Structural Journal*, V. 281, 2011, pp. 263-277.
16. Thiagarajan G, Johnson C.F., "Experimental behavior of reinforced concrete slabs subjected to shock loading", *ACI Structural Journal*, V. 111, No. 6, 2014, pp. 1407-1417.
17. Trasborg P., Nickerson J., Naito C., Olmati P., Davidson J., "Forming a predictable flexural mechanism in reinforced wall elements", *ACI Structural Journal*, V. 111, No. 6, 2014, pp. 1481-1490.
18. U.S. Army Corps of Engineers (USACE), "Methodology Manual for the Single-Degree-of-Freedom Blast Effects Design Spreadsheets (SBEDS)", 2008.
19. Wu C., Oehlers D.J., Rebentrost M., Leach J., Whittaker A.S., "Blast testing of ultra-high performance fibre and FRP-retrofitted concrete slabs", *Engineering Structures*, V. 31, 2009, pp. 2060-2069.
20. Zhou X.Q., Hao H., "Modelling of compressive behaviour of concrete-like materials at high strain rate", *International Journal of Solids and Structures*, V. 45, 2008, pp. 4648-4661.
21. Zineddin M., Krauthammer T., "Dynamic response and behavior of reinforced concrete slabs under impact loading", *International Journal of Impact Engineering*, V. 34, 2007, 1517-1534.

SIMULATION OF CONCRETE SLABS SUBJECTED TO BLAST USING THE COHESIVE CRACK MODEL

G. Morales-Alonso, D.A. Cendón and V. Sánchez-Gálvez

SYNOPSIS

Over recent years, numerical simulations have arisen as the most effective method to analyze structures under blast events. However, in order to achieve accurate numerical predictions, reliable constitutive models contrasted against experimental benchmarks are needed. In this work, the experimental tests on normal and high-strength concrete slabs conducted by the University Missouri-Kansas City on the shock tube at the Engineering Research and Design Center, U.S. Army Corps of Engineers at Vicksburg, Mississippi, are modeled by using a novel constitutive model for concrete presented recently by the authors. The model makes extensive use of Fracture Mechanics considerations through the Cohesive Crack Model developed by Hillerborg and co-workers. The numerical predictions obtained show good agreement with the experimental results, especially in the case of the high strength concrete slabs.

Keywords: blast loading; cohesive fracture; embedded crack; explosions; high strain rates; softening curve.

Biography:

Gustavo Morales-Alonso is an Assistant Professor at the Mechanical Engineering School of the Universidad Politécnica de Madrid (UPM). He received his MS in Civil Engineering and PhD from UPM, where he was a researcher at the Materials Science Department between 2009 and 2012. He has formerly been a research assistant at the Technical University of Munich (TUM, year 2004) and a visiting scholar at the Royal Institute of Technology in Stockholm (KTH, year 2012).

David A. Cendón is an Associate Professor at the Civil Engineering School of the Universidad Politécnica de Madrid, Spain (UPM). He received his PhD in Civil Engineering in 2002, and then joined the Materials Science Department where he carries out his research and teaching activities. He is the current secretary of the Spanish Society for Structural Integrity (Grupo Español de Fractura). He is the author of more 30 publications in SCI indexed journals.

Vicente Sánchez-Gálvez is a PhD in Civil Engineering and a MS in Physics. He is Full Professor at the Civil Engineering School of the Universidad Politécnica de Madrid, Spain (UPM). He has been the Dean of the Civil Engineering School, as well as the Vice-Rector of the Universidad Politécnica de Madrid. He is the author of 10 books, and over 200 papers in scientific journals.

INTRODUCTION

The design of buildings and other structures against blast loading has gained considerable attention from the community of engineers and architects. For many years, the amount of tools available for such purpose was scarce and usually too simplistic, like the recommendations and general indications that can be found in some manuals[1-3]. Later approaches were based on the use of simplified methodologies, such as the equivalent static load method[4] or the single degree-of-freedom technique[3]. Although being easy to use, these methodologies do not reflect the actual complexity of the problem, leading only to rough estimations of the true structural behavior.

The generalized use of computers during the last decades has changed this landscape and the use of numerical simulations has become the preferred tool for engineers that face the design and retrofit of structures subjected to blast loading. But the use of numerical simulations requires in turn for reliable material models if realistic predictions of the structural response are desired. This is only possible if adequate contrast of such models against experimental benchmarks involving blast testing[5-7] is conducted. In this paper, the experimental program conducted by the University Missouri-Kansas City at the Engineering Research and Design Center, U.S. Army Corps of Engineers at Vicksburg, Mississippi[7, 8] has been used to check the capabilities of a novel constitutive model for concrete under blast loading recently presented by the authors[9, 10].

Contrarily to most available material models in which the compressive response under high pressures is of the most importance, given that they were developed for ballistic purposes[11-13], in the model used in this work the emphasis is put on the tensile behavior. In quasi-brittle materials like concrete, such tensile behavior is responsible for crack initiation and the subsequent failure pattern that leads to the collapse of structural members. The model, which can be considered as a generalization for dynamic purposes of the one presented by Sancho[9, 10] for static loading has been adapted to hexahedral single integration point finite elements in order to be used in the LS-DYNA finite element code.

The results presented in this paper show that this model is capable of providing numerical predictions in good agreement with the experimental results, not only in the crack patterns registered in the tests, but also in the deflection histories measured for two different kind of concretes subjected to two different blast loads.

MATERIAL MODEL FOR CONCRETE

The material model used for concrete can be briefly described as a constitutive model with no failure under compression (linear-elastic behavior in the compressive domain), while failure in tension is modeled trough the Cohesive Crack Model once a threshold value for the maximum principal stress is exceeded. The cohesive crack is inserted in the finite elements through the *Embedded Crack Approach* (or *Strong Discontinuity Approach*).

The Cohesive Crack Model

Concrete is a quasi-brittle material that can be roughly considered to have a linear elastic behavior under mode I (pure tension) loading until it reaches its tensile strength. When the tensile strength is exceeded, damage appears in the material and the stresses that it can withstand are progressively reduced. This behavior can be approached through different constitutive models. In this research we rely on the *Cohesive Crack Model* (CCM), or *Fictitious Crack Model,* as presented by Hillerborg and coworkers[14], for which a numerical approach based on the *Embedded Crack Approach* was developed for static loading by a group of researchers leaded by Profs. Planas and Sancho[9, 10] belonging to the same research group presenting this contribution,. In the work presented here, the material model[9, 10] was enhanced for taking into account the effect of high strain rates by means of the *Dynamic Increase Factor* (DIF). Moreover, in order to allow for its implementation in the LS-DYNA finite element commercial software, it was necessary to adapt the material formulation for single integration point hexahedral elements. The implementation was made through a material user subroutine within the abovementioned finite element code.

In the CCM damage is assumed to concentrate in a discontinuity line, and, under mode I conditions (crack opening under pure tension) it is governed by a relationship between the crack opening, **w**, and the stress transmitted across the crack sides through a certain mathematical function, called softening curve (**Fig. 1**)[14, 15].

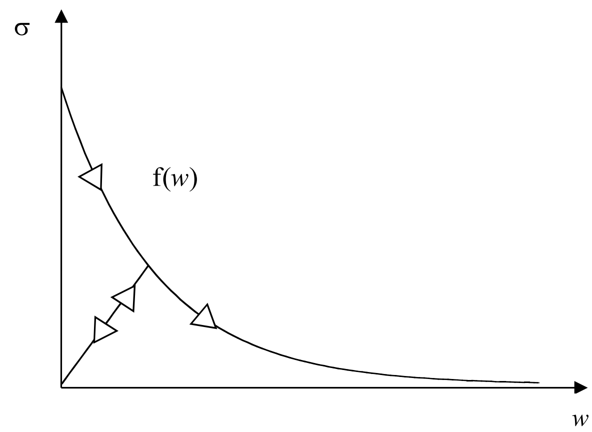

Fig. 1 - Softening curve.

To generalize to 3D mixed mode crack opening (combined tension and shear crack opening) the abovementioned mode I behavior, a central forces model has been used[9]. According to this central forces model, it is assumed that the traction vector **t** between crack borders is parallel to the crack displacement vector **w**, see **Fig. 2**. Therefore, the expression of the traction vector reads:

$$\mathbf{t} = \frac{f(\tilde{w})}{\tilde{w}} \cdot \mathbf{w} \qquad (1)$$

Where $\tilde{w} = \max(|\mathbf{w}|)$ is an equivalent crack opening value defined as the maximum registered opening in the crack and $f(\tilde{w})$ the softening function that relates the stress across the crack with crack opening.

In the absence of specific tests to determine the precise shape of the softening curve for the concrete types modeled here, the exponential one[15] has been chosen, although linear and bilinear approximations are also available in the model. The exponential approach is thought to be a good option for both its simplicity and the continuity of its derivatives. According to expression (1), unloading-reloading is assumed to follow a linear path, as shown in figure 1.

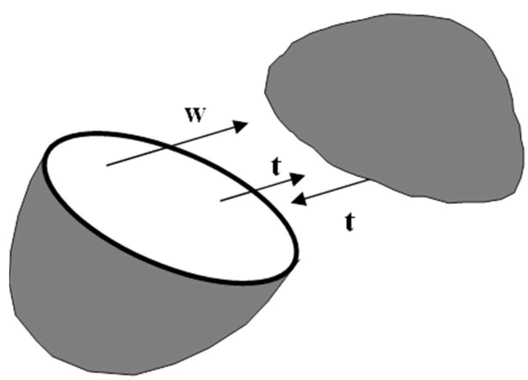

Fig. 2 - Central forces model.

<u>The embedded crack approach</u>

Equation (1) provides the traction vector **t** acting between both sides of the crack. However, in order to apply such traction, a crack must be first inserted somehow in the mesh. In order to address such issue without the need of defining beforehand the crack path, the *Embedded Crack Approach*[16, 17] was used.

The kinematics describing a strong discontinuity, such as a crack embedded on finite element, can be obtained by decoupling the displacement field into a continuous and a discontinuous part. In this decoupling the discontinuous part lumps the additional degrees of freedom related with the discontinuity, namely crack opening and sliding, which are incorporated through the displacement jump vector, **w**.

Let us consider a quite general finite element like the one depicted in **Fig. 3**. The element is crossed by a crack which divides it into the A^- and A^+ regions, as shown in the figure. The crack orientation is defined by the **n** vector, which is the unitary vector normal to the crack line. The jump in displacements is given by the **w** vector, which will be enforced to have a constant value along the crack embedded in the element. The equation[16] that describes the displacement field in the element under these conditions is given by:

$$\mathbf{u}(\mathbf{x}) = \sum_{\alpha \in A} N_\alpha(\mathbf{x}) \cdot \mathbf{u}_\alpha + \left[H(\mathbf{x}) - \sum_{\alpha \in A^+} N_\alpha(\mathbf{x}) \right] \cdot \mathbf{w} \quad (3)$$

Where α is the node index, $N_\alpha(x)$ is the shape function associated to node α, $\mathbf{u}_\alpha$ is the corresponding nodal displacement vector, **w** is the displacement jump vector and $H(\mathbf{x})$ is the Heaviside function ($H(\mathbf{x}) = 0$ if $\mathbf{x} \in A^-$; $H(\mathbf{x}) = 1$ if $x \in A^+$).

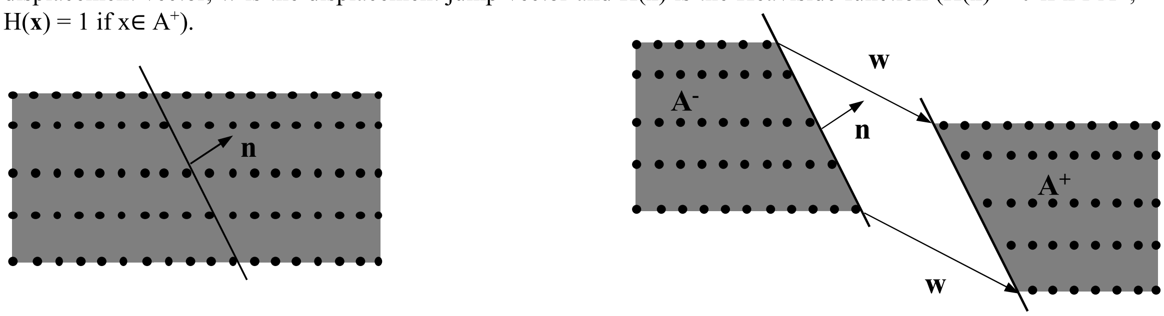

(a) (b)

Fig. 3 - Arbitrary finite element with (a) discontinuity line and (b) displacement jump through the discontinuity line.

The strain tensor can be obtained from the displacement field by taking the symmetric gradient to eqn. (3), leading to:

$$\boldsymbol{\varepsilon}^c(\mathbf{x}) = \sum_{\alpha \in A} \left[\mathbf{b}_\alpha(\mathbf{x}) \otimes \mathbf{u}_\alpha \right]^S - \left[\left(\sum_{\alpha \in A^+} \mathbf{b}_\alpha(\mathbf{x}) \right) \otimes \mathbf{w} \right]^S \quad (4)$$

where $\mathbf{b}_\alpha(\mathbf{x}) = \mathbf{grad}\ N_\alpha(\mathbf{x})$. In eqn. (4) the first term represents the strain field that would have the element if no displacement discontinuity were present on it, given that for this term the strain field is obtained from taking the derivative to the shape functions directly applied to the nodal displacements. For that reason, from now on we will name:

$$\boldsymbol{\varepsilon}^a(\mathbf{x}) = \sum_{\alpha \in A} \left[\mathbf{b}_\alpha(\mathbf{x}) \otimes \mathbf{u}_\alpha \right]^S \quad (5)$$

in which the superscript *a* stands for apparent. The second term in eqn. (4) represents the amount that must be subtracted to the apparent strains in order to take into account for the presence of the crack. For the sake of simplicity, we will adopt the following notation:

$$\mathbf{b}^+(\mathbf{x}) = \sum_{\alpha \in A^+} \mathbf{b}_\alpha(\mathbf{x}) \quad (6)$$

Therefore, the $\mathbf{b}^+$ vector is obtained as the sum of the gradients of the shape functions corresponding to the nodes belonging to the A^+ region. From now on, these nodes will be referred to as *solitary nodes*. Consequently, the choice of the solitary nodes becomes a key issue in the formulation of the embedded crack model, since they determine the kinematics of the model. By substituting eqns. (5) and (6) in (4), we obtain:

$$\boldsymbol{\varepsilon}^{c}(\mathbf{x}) = \boldsymbol{\varepsilon}^{a}(\mathbf{x}) - \left[\mathbf{b}^{+}(\mathbf{x}) \otimes \mathbf{w}\right]^{S} \qquad (7)$$

Initiation and orientation of the crack

Maximum principal stress is used to obtain both the crack initiation and the crack orientation. Once the maximum principal stress overcomes the tensile strength, a crack is introduced perpendicular to the direction of the former. Therefore the crack orientation **n** is computed as the unit eigenvector associated to such maximum principal stress. In principle, for a given element, there should be as many principal stress directions as integration points were present in the element. This issue is circumvented by applying this methodology only to constant stress elements[9, 10]. For the model developed here, 3D hexahedral single integration point elements have been used.

However, by setting the crack direction the problem of deciding which are the solitary nodes is not solved. **Fig. 4** shows some of the possible solitary nodes combinations for a given crack direction associated to a certain **n** vector.

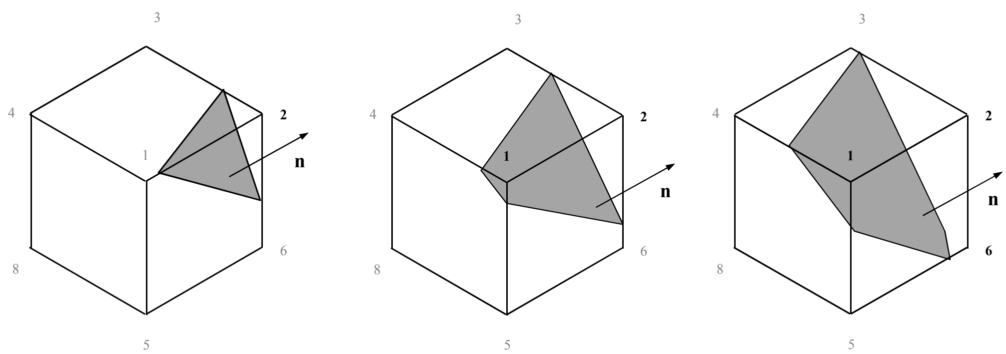

Fig. 4 - Examples of some of the different solitary nodes combinations for a unique crack orientation when varying its position, where the solitary nodes are printed in bold letters.

Among all the possible combinations of solitary nodes and, subsequently of possible $\mathbf{b}^{+}$ vectors, in this work the solitary nodes are determined by requiring that the angle between vectors **n** and $\mathbf{b}^{+}$ is the smallest possible[9, 18]:

$$\frac{\mathbf{n} \cdot \mathbf{b}^{+}}{\left|\mathbf{b}^{+}\right|} = \max \qquad (8)$$

All this procedure of calculating **n** and $\mathbf{b}^{+}$ takes place locally every time a finite element exceeds the maximum principal stress criterion and no crack continuity is enforced between adjacent elements. At first stages of the crack development, stress waves in the material may cause an element to crack on a direction significantly different to the one in the adjacent element pre-existing crack, thus producing an undesirable crack locking effect. To avoid this problem without introducing complex crack continuity algorithms, the concept of crack adaptation[9], is adopted here. This approach allows the crack to adapt itself to later variations of its principal stress direction while its opening does not overcome a certain threshold value. Once such value is exceeded, the crack direction is frozen. For the simulations presented here, the value of $w_{adapt}=0.1 \cdot G_F/f_t$ has been chosen, being w_{adapt} the threshold crack opening value, G_F the specific fracture energy, and f_t the tensile strength.

The use of hexahedral elements instead of the tetrahedrons offers two major advantages. First of all, the whole element presents more possible combinations of solitary nodes and, subsequently, more possible $\mathbf{b}^{+}$ vectors to find the more parallel one to the **n** direction, following eqn. (8). This fact provides an element kinematics more compliant with the crack orientation, according to the maximum principal stress criterion, and therefore a better description of the crack kinematics.

The second advantage appears when a structured mesh is used. Since the $\mathbf{b}^{+}$ vector is obtained as the gradient of the shape functions corresponding to the solitary nodes, global coordinates of these nodes would be required to obtain such vector. Many commercial explicit codes, such as LS-DYNA or AUTODYN, do not allow user programmed elements and only material user subroutines are available. Unfortunately, nodal coordinates are not usually accessible at the material level (integration point level). However in case of using a structured mesh of hexahedral elements, for all the elements present in the model the eight shape functions of all elements are equal eight to eight with the only difference of being translated in the XYZ space. Since the $\mathbf{b}^{+}$ vector comes from the gradient of the shape functions and the spatial translation does not affect the result of the gradient, all the possible $\mathbf{b}^{+}$ vectors for all elements are exactly the same. Then, the only required parameters are the lengths of the hexahedra sides, which can be input to the subroutine as any other material property. This strategy makes possible the use of this material model in a wide variety of commercial and non commercial numerical codes. The only price to pay is that nodal positions cannot be obviously updated and therefore it is only suitable for small displacement analyses.

Local equilibrium

As it has been aforementioned, the material behaves as linear elastic until the maximum principal stress exceeds the threshold value of the tensile strength. At this moment the cohesive crack is embedded in the element. Since outside the crack the material continues behaving linear elastic, we can obtain the stress tensor by applying:

$$\boldsymbol{\sigma} = \mathbf{D} \cdot \boldsymbol{\varepsilon}^{\mathbf{c}} \qquad (9)$$

being $\mathbf{D}$ the elastic moduli fourth order tensor. By substituting $\boldsymbol{\varepsilon}^{\mathbf{c}}$ by its value according to eqn. (7), now it reads:

$$\boldsymbol{\sigma} = \mathbf{D} \cdot \left[\boldsymbol{\varepsilon}^{\mathbf{a}} - \mathbf{b}^{+} \otimes \mathbf{w}\right]^{S} \qquad (10)$$

The previous expression provides Cauchy's stress tensor in the continuum part of the element. However the traction vector acting along the crack sides must satisfy local equilibrium with the abovementioned stress tensor. In other words, the traction vector corresponding to the $\mathbf{n}$ direction applied to Cauchy's tensor of the continuum must be equal to the crack's traction vector, given by (1):

$$\mathbf{t}_{\mathbf{crack}} = \frac{f(\tilde{w})}{\tilde{w}} \cdot \mathbf{w} \qquad (11)$$

$$\mathbf{t}_{\mathbf{continuum}} = \left(\mathbf{D} \cdot \boldsymbol{\varepsilon}^{\mathbf{c}}\right) \cdot \mathbf{n} = \left[\mathbf{D} \cdot \boldsymbol{\varepsilon}^{\mathbf{a}} - \mathbf{D} \cdot \left[\mathbf{b}^{+} \otimes \mathbf{w}\right]^{S}\right] \cdot \mathbf{n} \qquad (12)$$

$$\mathbf{t}_{\mathbf{crack}} = \mathbf{t}_{\mathbf{continuum}} \rightarrow \quad \frac{f(\tilde{w})}{\tilde{w}} \cdot \mathbf{w} = \mathbf{D} \cdot \left[\boldsymbol{\varepsilon}^{\mathbf{a}} - \left[\mathbf{b}^{+} \otimes \mathbf{w}\right]^{S}\right] \cdot \mathbf{n} \qquad (13)$$

Equation (13) is the basic equation governing the cohesive embedded crack formulation. In the equation, the only unknown is the crack displacements vector, $\mathbf{w}$, and must be solved by numerical methods.

Rate effects

In a reinforced concrete element subjected to a blast event the load is applied at a very high strain rate[19, 20], within the order of 10 s^{-1} to 1000 s^{-1}. While the mechanical properties of almost all materials are strain rate sensitive, the effect of high strain rates is particularly remarkable in the case of concrete.

The most usual way of taking into account the effect of strain rates is through the Dynamic Increase Factor (DIF), which is obtained as the ratio between the dynamic and the static strength. The DIF is normally defined for the compressive strength and the tensile strength[20, 21].

Some attempts have been also made to obtain the DIF for the fracture energy of concrete[22-24]. Although the experimental data are scarce, it seems that the DIF for fracture energy could be similar to the DIF for the tensile strength. Therefore, in this research a multiplicative formulation is proposed to take into account for rate effects. It consists on multiplying the whole softening curve by the DIF, as shown in **Fig. 5**. As a result, both the tensile strength and the fracture energy are simultaneously increased by the same factor, in line with the experimental results obtained by Weerheijm[23]. The expression of the DIF applied in this research is the one provided for the tensile strength by the CEB Bulletin 187[21]:

$$DIF = \frac{f_{td}}{f_{ts}} = \left[\frac{\dot{\varepsilon}}{\dot{\varepsilon}_0}\right]^{1.016\delta} \quad \text{for } \dot{\varepsilon} \leq 30\,s^{-1}$$

$$DIF = \frac{f_{td}}{f_{ts}} = \eta \cdot \left[\frac{\dot{\varepsilon}}{\dot{\varepsilon}_0}\right]^{\frac{1}{3}} \quad \text{for } \dot{\varepsilon} > 30\,s^{-1} \qquad (16)$$

Where $\delta = \dfrac{1}{10 + 6 \cdot f_{ts}}$ and $\eta = 10^{7.11 \cdot \delta - 2.33}$, f_{td} and f_{ts} are the dynamic and static tensile strengths of concrete, respectively, f_{cs} is the static compressive strength of concrete, $\dot{\varepsilon}$ is the actual strain rate and $\dot{\varepsilon}_0$ is the static strain rate, which is taken as $3 \cdot 10^{-6}$ s^{-1}.

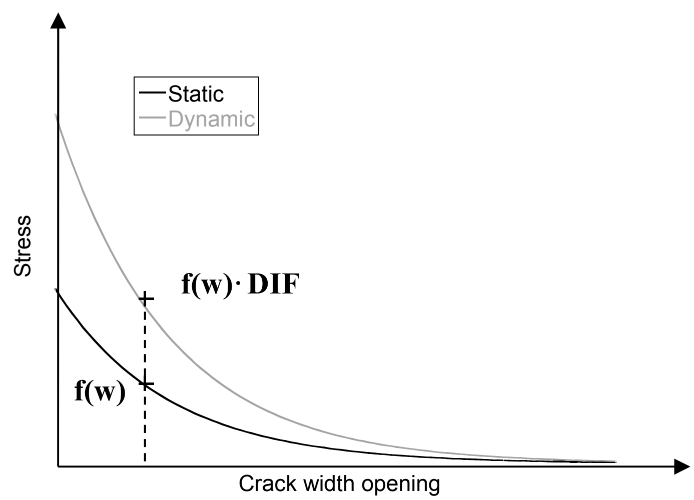

Fig. 5 - Exponential softening function original and enhanced due to strain rate.

Material parameters used for the concretes

The material properties of concrete have been obtained from graphics and data given by Thiagarajan[7]. Some of the material properties were explicitly given, and others had to be deducted. It is worthy to note that no information was provided regarding the tensile behavior of both concrete types. Therefore, the values of the tensile strength, specific fracture energy and shape of the softening curve of concrete had to be estimated, since, as shown in the previous section, the material model proposed only takes into account failure under tension. The estimated material properties were obtained to according to the engineering expressions provided by Model Code 2010[25].

Table 1 summarizes the mechanical properties of the materials involved in the experimental campaign. Since the original data were given in Imperial units, they have been transformed into International System units. As no information was provided regarding concrete softening curve, it has been assumed that the exponential curve would represent the softening behavior accurately. This is the most commonly used softening curve in the commercial software that simulate the fracture of concrete.

Table 1–Mechanical properties of concrete used in the simulations

Mechanical property	NSC	HSC
Density [kg/m^3]	2350	2368

Young's modulus [GPa]	33.33	40.78
Poisson's ratio [-]	0.20*	0.26
Tensile strength [MPa]	4.00*	6.00*
Fracture energy [N·m]	100*	120*
Softening curve	Exponential	Exponential
Yield stress [MPa]	-	-
Tangent Young's modulus [GPa]	-	-

Note: Values marked with * have been estimated with the use of Model Code 2010[25] from the data given by Thiagarajan[7].

MATERIAL MODEL FOR STEEL REBARS

The Johnson-Cook model

The constitutive model used for steel rebars has been the Johnson-Cook material model[26] developed for metals under high strain rates. This is a widely used model, which is based on a classical J_2 plasticity model with a yield surface that is scaled depending on the effect of temperature and strain rate. The formulation of the yield surface splits into three different terms: the strain hardening of the material, the strain rate hardening and the thermal softening, which are considered independently. According to this model, the yield stress of the material is given by:

$$Y_{JC} = \left[A + B \cdot \varepsilon_p^n\right] \cdot \left[1 + C \cdot \ln \dot{\varepsilon}_p^*\right] \cdot \left[1 - T^{*m}\right] \qquad (17)$$

Material parameters used for the steel

The mechanical properties of steel rebars (see **Table 2**) have been taken from Thiagarajan[7], while the Johnson-Cook parameters have been estimated with the values proposed in Magnusson[27].

Table 2–Mechanical properties of steel used in the simulations

Mechanical property	NSS	HSS
Density [kg/m^3]	7850	7850
Young's modulus [GPa]	200	200
Poisson's ratio [-]	0.30*	0.30*
Tangent Young's modulus [GPa]	4.25	3.20
Input constant A for strain hardening [GPa]	0.482	0.565
Input constant B for strain hardening [GPa]	0.00	0.00
Input constant n for strain hardening	0.01	0.01
Input constant C for strain rate hardening	0.025	0.025
Input constant m for thermal softening	0.00	0.00